Structural basis for the acyl chain selectivity and mechanism of UDP-*N*-acetylglucosamine acyltransferase

Allison H. Williams and Christian R. H. Raetz*

Department of Biochemistry, Duke University Medical Center, Box 3711 DUMC, Durham, NC 27710

This contribution is part of the special series of Inaugural Articles by members of the National Academy of Sciences elected on April 25, 2006.

Contributed by Christian R. H. Raetz, June 21, 2007 (sent for review May 10, 2007)

UDP-*N*-acetylglucosamine (UDP-GlcNAc) acyltransferase (LpxA) catalyzes the first step of lipid A biosynthesis, the reversible transfer of the *R*-3-hydroxyacyl chain from *R*-3-hydroxyacyl acyl carrier protein to the glucosamine 3-OH group of UDP-GlcNAc. *Escherichia coli* LpxA is highly selective for *R*-3-hydroxymyristate. The crystal structure of the *E. coli* LpxA homotrimer, determined previously in the absence of lipid substrates or products, revealed that LpxA contains an unusual, left-handed parallel β-helix fold. We have now solved the crystal structures of *E. coli* LpxA with the bound product UDP-3-*O*-(*R*-3-hydroxymyristoyl)-GlcNAc at a resolution of 1.74 Å and with bound UDP-3-*O*-(*R*-3-hydroxydecanoyl)-GlcNAc at 1.85 Å. The structures of these complexes are consistent with the catalytic mechanism deduced by mutagenesis and with a recent 3.0-Å structure of LpxA with bound UDP-GlcNAc. Our structures show how LpxA selects for 14-carbon *R*-3-hydroxyacyl chains and reveal two modes of UDP binding.

UDP-3-*O*-(*R*-3-hydroxymyristoyl)-acetylglucosamine | acyl carrier protein | LpxA | *Escherichia coli* | x-ray crystallography

The Kdo_2-lipid A substructure (Fig. 1) of LPS is required for the growth of most Gram-negative bacteria and accounts for the some of the toxic side-effects of Gram-negative sepsis (1–4). In *Escherichia coli*, UDP-*N*-acetylglucosamine (UDP-GlcNAc) acyltransferase (LpxA) catalyzes the first step of lipid A biosynthesis (5–7), the reversible transfer of the *R*-3-hydroxymyristoyl moiety from *R*-3-hydroxymyristoyl-acyl carrier protein (ACP) to the glucosamine 3-OH group of UDP-GlcNAc (Fig. 1) (8). Because LpxA catalyzes a thermodynamically unfavorable reaction ($K_{eq} \approx 0.01$) (8), the second enzyme of the pathway, the deacetylase (LpxC), is the committed step (9, 10). LpxA and LpxC are essential for growth (10–12), and both are validated targets for the design of novel antibiotics (13–15).

UDP-GlcNAc acyltransferases are soluble cytoplasmic proteins (8, 16, 17). They usually require *R*-hydroxyacyl-ACP as donor substrates (6, 8, 18). Although highly selective for *R*-3-hydroxymyristoyl-ACP, *E. coli* LpxA utilizes *R*-3-hydroxylauroyl-ACP and *R*-3-hydroxypalmitoyl-ACP at 1–2% the rate of *R*-3-hydroxymyristoyl-ACP under standard assay conditions (6, 18, 19). *R*-3-hydroxydecanoyl-ACP is used at ≈0.1% the rate of *R*-3-hydroxymyristoyl-ACP (18, 19). *Pseudomonas aeruginosa* LpxA is maximally active with *R*-3-hydroxydecanoyl-ACP, which it prefers over *R*-3-hydroxymyristoyl-ACP by a factor of 1,000 (18–20). The *in vitro* fatty acyl chain length selectivity of these LpxA orthologues is consistent with the structures of the lipid A molecules isolated from *E. coli* and *P. aeruginosa* (2). The only known LpxA variant that does not require *R*-3-hydroxyacyl-ACP is that of *Chlamydia trachomatis*, which shows a strong preference for myristoyl-ACP over *R*-3-hydroxymyristoyl-ACP (21). *E. coli* LpxA is inhibited by myristoyl-ACP (8).

The crystal structure of *E. coli* LpxA was first determined in 1995 at a resolution of 2.6 Å in the absence of substrates or inhibitors (16). A structure of *Helicobacter pylori* LpxA with a bound molecule of 1-*S*-octyl-β-thio-D-glucoside was subsequently determined at 2.1 Å (17). Both LpxAs are homotrimers with an unusual secondary structure, a left-handed parallel β-helix (16, 17), which is generated by 30 hexapeptide repeats. Three contiguous hexad repeats specify one turn of the β-helix (16). Several other bacterial acetyl and acyl transferases, including DapD (22), GlmU (23), and LacA (24), share similar repeats and possess β-helical domains, as do a few archaebacterial (25) and eukaryotic proteins (26).

Sequence alignments of LpxAs from diverse bacteria reveal many conserved basic residues, including several histidine residues (18), which cluster around a cleft in between adjacent subunits, and they function in substrate binding and catalysis (18). H125 was proposed to be the catalytic base that activates the GlcNAc 3-OH group, facilitating the direct transfer of the acyl chain from *R*-3-hydroxymyristoyl-ACP (18). A H125A substitution results in complete loss of activity (18). A recent 3.0-Å crystal structure of *E. coli* LpxA with bound UDP-GlcNAc confirmed that H125 is within hydrogen-bonding distance of the 3-OH group (27). H122, H144, H160, and R204 were proposed to be involved in substrate binding, because alanine substitutions reduced but did not eliminate activity (18). In the LpxA/UDP-GlcNAc complex, H144 is positioned to hydrogen-bond the 6-OH group of the GlcNAc moiety, and R204 contacts the α-P atom of UDP (27).

G173 strongly influences acyl chain selectivity (19) and may function as a kind of hydrocarbon ruler. The G173M mutant of *E. coli* LpxA prefers *R*-3-hydroxydecanoyl-ACP, whereas activity with *R*-3-hydroxymyristoyl-ACP is lost (19). The reciprocal M169G mutation of *P. aeruginosa* LpxA converts what is normally an *R*-3-hydroxydecanoyl-ACP-selective enzyme to an *R*-3-hydroxymyristoyl-ACP-selective enzyme (19). *H. pylori* LpxA prefers 16 carbon *R*-3-hydroxyacyl chains (C. R. Sweet and C.R.H.R., unpublished data).

We recently described the structure of *E. coli* LpxA with the bound inhibitor peptide 920 (28), which binds in a region overlapping with *R*-3-hydroxymyristoyl-ACP. Peptide 920 does not share sequence similarity with ACP or LpxA (28, 29). The structures of the LpxA/peptide 920 (28) and the LpxA/UDP-GlcNAc (27) complexes did not reveal how LpxA acquires its extraordinary acyl chain selectivity. Attempts to crystallize LpxA with acyl-ACP have been unsuccessful, but crystallization of LpxA with its product UDP-3-*O*-(*R*-3-hydroxymyristoyl)-

Author contributions: A.H.W. and C.R.H.R. designed research; A.H.W. performed research; A.H.W. contributed new reagents/analytic tools; A.H.W. and C.R.H.R. analyzed data; and A.H.W. and C.R.H.R. wrote the paper.

The authors declare no conflict of interest.

Data deposition: The atomic coordinates and structure factors have been deposited in the Protein Data Bank, www.pdb.org (PDB ID codes 2QIA and 2QIV).

*To whom correspondence should be addressed. E-mail: raetz@biochem.duke.edu.

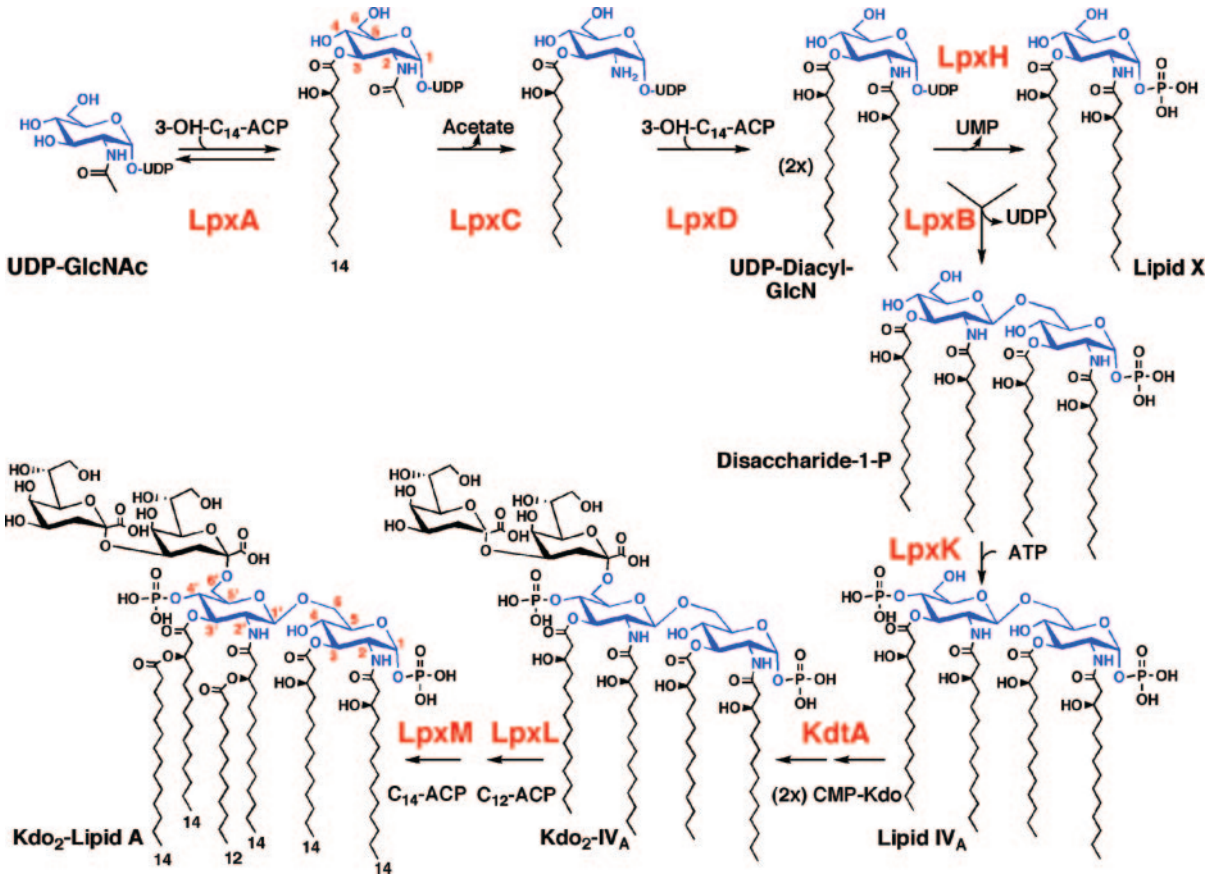

Fig. 1. Functions of LpxA and LpxC in lipid A biosynthesis. LpxA catalyzes the first step, the acylation of UDP-GlcNAc (2, 4). This is a thermodynamically unfavorable reaction; therefore, LpxC catalyzes the committed step of the pathway (8).

GlcNAc (6, 8) had not been investigated. Here we present the crystal structures of LpxA with bound UDP-3-*O*-(*R*-3-hydroxymyristoyl)-GlcNAc at a resolution of 1.74 Å and UDP-3-*O*-(*R*-3-hydroxydecanoyl)-GlcNAc at 1.85 Å. As in the 3.0-Å LpxA/UDP-GlcNAc complex (27), H125 is within hydrogen-bonding distance of the GlcNAc 3-*O* atom. The positioning of G173 relative to the terminal methyl group of the *R*-3-hydroxymyristoyl chain explains why the LpxA G173M mutation is *R*-3-hydroxydecanoyl-ACP-selective and why the G173S and the G173C substitutions cannot use *R*-3-hydroxymyristoyl- or *R*-3-hydroxylauoryl-ACP (19). Specific roles for H99, H122, H144, K76, Q73, Q161, R204, and R205 are apparent from our structures. Although the positioning of the GlcNAc moiety is identical in both the LpxA/UDP-3-*O*-(*R*-3-hydroxymyristoyl)-GlcNAc and the LpxA/UDP-3-*O*-(*R*-3-hydroxydecanoyl)-GlcNAc complexes, the conformation of the UDP moiety is distinctly different.

Results

Structure of LpxA with Bound UDP-3-*O*-(*R*-3-hydroxyacyl)-GlcNAc. The LpxA reaction is reversible, with the equilibrium favoring the reactants over products ($K_{eq} \approx 0.01$) (8, 18). Consequently, LpxA catalyzes the efficient deacylation of UDP-3-*O*-(*R*-3-hydroxymyristoyl)-GlcNAc in the presence of ACP to yield UDP-GlcNAc and *R*-3-hydroxymyristoyl-ACP (8, 18). *E. coli* LpxA does not hydrolyze UDP-3-*O*-(*R*-3-hydroxyacyl)-GlcNAc in the absence of ACP (8, 18). The enzyme was therefore crystallized in the presence of a 25-fold molar excess of either UDP-3-*O*-(*R*-3-hydroxymyristoyl)-GlcNAc or UDP-3-*O*-(*R*-3-hydroxydecanoyl)-GlcNAc. The crystals of UDP-3-*O*-(*R*-3-hydroxymyristoyl)-GlcNAc diffracted to a resolution of 1.74 Å, whereas crystals of UDP-3-*O*-(*R*-3-hydroxydecanoyl)-GlcNAc diffracted to 1.85 Å. The structures of both complexes were solved by molecular replacement, using unliganded LpxA (Protein Data Bank ID code 1LXA) as the model (16). The asymmetric unit of both complexes was composed of one LpxA monomer with one bound UDP-3-*O*-(*R*-3-hydroxyacyl)-GlcNAc molecule. Three asymmetric units are positioned around a crystallographic threefold axis to form the biologically relevant trimer (Fig. 2) (16). In both complexes, >98% of all amino acid residues were in favored regions of the Ramachandran plot, as determined by Molprobity (30). The data collection and refinement statistics are presented in Table 1.

Examination of both structures reveals that the complexes possess the same left-handed parallel β-helix architecture (Fig. 2) described for unliganded LpxA (16). The bound products did not cause major conformational changes. Superposition of unliganded LpxA with LpxA/UDP-3-*O*-(*R*-3-hydroxymyristoyl)-GlcNAc or with LpxA/UDP-3-*O*-(*R*-3-hydroxydecanoyl)-GlcNAc revealed an average rmsd of 0.37 and 0.34 Å, respectively, for all paired C^{α} atoms. The perturbation of the side-chains was generally very minor (0.2 Å) but was more significant for some of the residues located near the ligands. In particular, the acyl chains of the ligands displaced the side chain of H160 when compared with free LpxA or the LpxA/UDP-GlcNAc complex. Superimposition of the LpxA/UDP-3-*O*-(*R*-3-hydroxymyristoyl)-GlcNAc complex and the LpxA/UDP-3-*O*-(*R*-3-hydroxydecanoyl)-GlcNAc complex gave an rmsd of 0.10 Å for all C^{α} pairs of the backbone. In both structures, the electron density of LpxA was clear and consistent for all 262 amino acids (data not shown).

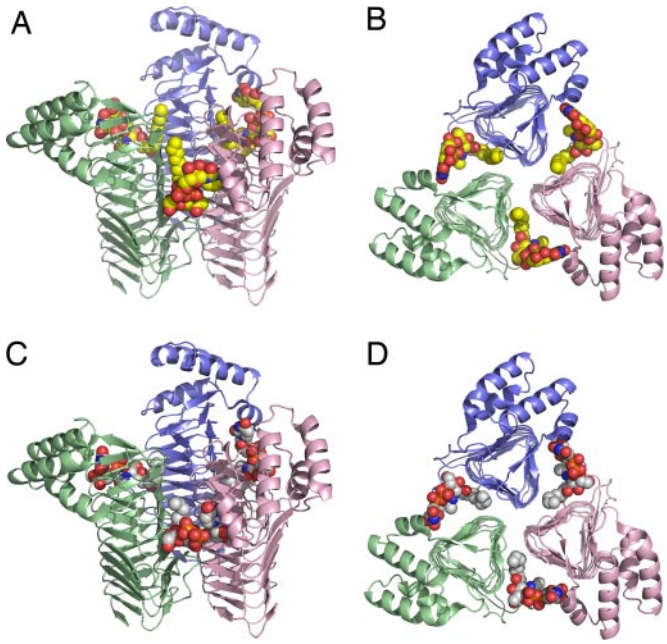

Fig. 2. Structural models of two LpxA/product complexes. (*A*) Side view of LpxA (ribbon diagram) with UDP-3-*O*-(*R*-3-hydroxymyristoyl)-GlcNAc (space filling model) at a resolution of 1.74 Å. Individual monomers of the LpxA homotrimer are colored green, magenta, and blue. The UDP-3-*O*-(*R*-3-hydroxymyristoyl)-GlcNAc product binds within the active site region located between adjacent subunits, as anticipated from site-directed mutagenesis studies (18). In the space-filling model of the ligand, carbon is yellow, nitrogen is blue, oxygen is red, and phosphorus is orange. (*B*) The top-down view demonstrates the threefold symmetry of the bound ligand. (*C*) The side view of LpxA (ribbon diagram) with bound UDP-3-*O*-(*R*-3-hydroxydecanoyl)-GlcNAc (space-filling model) at a resolution of 1.85 Å. The color scheme is similar to that described in *A*, except that the carbon atoms of the *R*-3-hydroxydecanoyl chain are gray. (*D*) Top-down view of the LpxA/UDP-3-*O*-(*R*-3-hydroxydecanoyl)-GlcNAc complex.

UDP-3-*O*-(*R*-3-hydroxymyristoyl)-GlcNAc and UDP-3-*O*-(*R*-3-hydroxydecanoyl)-GlcNAc bind to *E. coli* LpxA in similar, but not identical, conformations (Fig. 2, compare *A* and *B* with *C* and *D*, respectively). Each active site region accommodates one molecule of UDP-3-*O*-(*R*-3-hydroxyacyl)-GlcNAc (Fig. 2). The electron densities of the UDP-3-*O*-(*R*-3-hydroxymyristoyl)-GlcNAc and UDP-3-*O*-(*R*-3-hydroxydecanoyl)-GlcNAc were well resolved (Fig. 3 *A* and *B*, respectively). Strong electron density was observed in both cases for the glucosamine ring, the acyl and acetyl chains, the phosphate residues, and the uracil moiety. The density for the ribose unit was weaker, especially in the case of UDP-3-*O*-(*R*-3-hydroxymyristoyl)-GlcNAc (Fig. 3*A*). The tail of the electron density leading away from the β-phosphate moiety in Fig. 3*A* suggests the possibility that a small portion of the bound UDP-3-*O*-(*R*-3-hydroxymyristoyl)-GlcNAc may be in the alternative conformation seen for UDP-3-*O*-(*R*-3-hydroxydecanoyl)-GlcNAc.

UDP-3-*O*-(*R*-3-hydroxymyristoyl)-GlcNAc in the Active Site of LpxA. Each molecule of UDP-3-*O*-(*R*-3-hydroxymyristoyl)-GlcNAc interacts with residues from two adjacent LpxA subunits. As illustrated in Fig. 4*A*, the glucosamine ring and the 3-*O*-(*R*-3-hydroxymyristoyl) moiety are positioned next to the green subunit, whereas the UDP moiety extends toward the adjacent magenta subunit. The 3-OH group of the glucosamine ring is buried. The fatty acyl chain extends from the 3-*O* atom into the active site cleft along the green subunit. The first four carbon atoms are almost perpendicular to the long axis of the β-helix (Figs. 2*B* and 4*A*). The rest of the hydrocarbon chain runs parallel to the β-helix (Figs. 2*A* and 4*A*). The approximate length of the 3-*O*-(*R*-3-hydroxymyristoyl) chain is 14 Å. The phosphates of the UDP moiety are solvent exposed.

UDP-3-*O*-(*R*-3-hydroxymyristoyl)-GlcNAc is supported in the active site of LpxA by multiple hydrogen bonds to conserved side chains (Fig. 4*A*), some of which were previously identified by mutagenesis as being involved in catalysis or substrate binding (18, 19). Thirteen water molecules directly interact with the ligand. Ten of them are within hydrogen-bonding distance of the UDP moiety, and two of them hydrogen-bond the GlcNAc residue. A single water molecule interacts with the *R*-3-OH group of the hydroxyacyl chain in an intricate network that also engages several conserved amino acid residues (Fig. 4*A*). H125 is within hydrogen-bonding distance of the GlcNAc 3-*O* atom (Fig. 4*A*), consistent with its role as the catalytic base (18). H122 and Q73 hydrogen-bond the *R*-3-OH group of the acyl chain; one well defined water molecule also hydrogen-bonds the *R*-3-OH group, and it forms an additional bond to H99 (Fig. 4*A*). H144 and K76 (not shown for clarity) are hydrogen-bonded to the GlcNAc 6-OH group (Fig. 4*A*), consistent with their location in the LpxA/UDP-GlcNAc complex. K76 also interacts with *O*-5 of the GlcNAc unit. The backbone nitrogen of L76 is hydrogen-bonded to the acetyl group of the glucosamine ring (Fig. 4*A*). The conserved Q161 side chain is hydrogen-bonded to two oxygen atoms, one on each of the phosphate residues. N198 and R205 are hydrogen-bonded to the uridine moiety (Fig. 4*A*). R204 and D74 (not shown) are involved in water-mediated interactions with the ligand.

UDP-3-*O*-(*R*-3-hydroxydecanoyl)-GlcNAc in the Active Site of LpxA. Comparison of the LpxA/UDP-3-*O*-(*R*-3-hydroxydecanoyl)-GlcNAc complex with the LpxA/UDP-3-*O*-(*R*-3-hydroxymyristoyl)-GlcNAc complex revealed striking similarities and differences in the binding of the ligands (Figs. 4 and 5*A*). The GlcNAc unit, the first four carbons of the fatty acyl chain, and the β-phosphate group superimpose very well (Figs. 4 and 5*A*). However, the α-phosphate group and the ribose ring assume different orientations, which nevertheless allow the uracil moiety to hydrogen-bond to the N198 side chain (Figs. 4 and 5*A*). These observations, in conjunction with the relatively weak electron density of the ribose units (Fig. 3), suggest some flexibility of the UDP moiety, which is influenced by the length of the acyl chain. As shown in Fig. 5*B*, the conformation of the UDP-GlcNAc unit in the LpxA/UDP-3-*O*-(*R*-3-hydroxydecanoyl)-GlcNAc complex is virtually the same as in the 3-Å LpxA/UDP-GlcNAc complex (27).

Most of the interactions between the ligands and LpxA are the same in both of our structures (Fig. 4, compare *A* with *B*). For example, H125 is within hydrogen-bonding distance of the GlcNAc 3-*O* atom in both cases (Fig. 4). In addition, H122, H144, H99, K76, Q73 L76, D74, Q161, N198, and R205 are all similarly involved in substrate binding, with the exception of R204, which is directly hydrogen-bonded to the α-phosphate of UDP-3-*O*-(*R*-3-hydroxydecanoyl)-GlcNAc (Fig. 4*B*) but not UDP-3-*O*-(*R*-3-hydroxymyristoyl)-GlcNAc (Fig. 4*A*). The pattern of water molecules interacting with the GlcNAc and *R*-3-OH group is identical, but there are differences around the UDP moiety (Fig. 4, compare *A* with *B*). The backbone N atom of the conserved G143 residue is situated 3.32–3.35 Å from the carbonyl oxygen of the hydroxyacyl chain (Fig. 4). It may be positioned to function as the oxyanion hole during catalysis.

Acyl Chain Selectivity of *E. coli* LpxA. Previous studies identified G173 as being involved in acyl chain length recognition (19). The *E. coli* LpxA G173M mutant and the reciprocal *P. aeruginosa* LpxA M169G mutant showed reversed acyl chain length selectivity *in vitro* and *in vivo* (19). *E. coli* LpxA G173M is an *R*-3-hydroxydecanoyl-ACP-selective acyltransferase, whereas *P. aeruginosa* LpxA M169G is an *R*-3-hydroxymyristoyl-ACP-

Table 1. Data collection and refinement statistics of *E. coli* LpxA with bound lipid products

Parameter	LpxA/UDP-3-*O*-(*R*-3-hydroxydecanoyl)-GlcNAc	LpxA/UDP-3-*O*-(*R*-3-hydroxymyristoyl)-GlcNAc
Source/detector	RU200/R-Axis IV	RU200/R-Axis IV
Space group	$P2_13$	$P2_13$
$a = b = c$, Å	97.14	96.72
Wavelength, Å	1.5418	1.5418
Resolution range,* Å	21.65–1.85	23.6–1.74
Last shell, Å	1.85–1.89	1.74–1.78
Unique reflections	22,884	28,527
Completeness, % (last shell)	98.3 (98.7)	96.5 (93.1)
Average $I/s_{(I)}$ (last shell)	17.6 (3.4)	35.5 (5.5)
Redundancy (last shell)	3.3 (3.5)	4.6 (4.7)
R_{merge},† %	5.0	4.7
Nonsolvent atoms		
Protein	1,974	1,974
Product	50	54
Solvent atoms	368	434
rmsd from ideality		
Bond lengths, Å	0.006	0.007
Bond angles, °	1.049	1.093
R value‡	19.6	18.7
R_{free}‡	22.3	23.0
All-atom clash score	3.0	4.25

*Resolution limit was defined as the highest resolution shell where the average I/σ_I was 2.
†$R_{merge} = \Sigma_{hkl}\Sigma_i|I_i(hkl) - \langle I_{(hkl)}\rangle|/\Sigma_{hkl}\Sigma_i I_{(hkl)}$.
‡$R = \Sigma|F_o - F_c|/\Sigma F_o$. Five percent of the reflections was used to calculate R_{free}.

specific enzyme (19). *E. coli* LpxA G173 is located on the magenta subunit, opposite the green subunit that supplies H125 (Figs. 4 and 6). The acyl chain of UDP-3-*O*-(*R*-3-hydroxymyristoyl)-GlcNAc (yellow dots) extends deep into the active site cleft, passing by G173 and G176 (Fig. 6). The acyl chain of UDP-3-*O*-(*R*-3-hydroxydecanoyl)-GlcNAc (not shown) terminates below G173, approximately where C9 of the *R*-3-hydroxymyristoyl chain would be situated (Fig. 5). Replacing G173 with methionine would be expected to leave enough space for a 3-hydroxydecanoyl chain but would result in a clash with a 3-hydroxymyristoyl chain. The G173M substitution might increase the affinity of the enzyme for *R*-3-hydroxydecanoyl-ACP (19) by providing extra hydrophobic contacts to the terminal methyl group of the *R*-3-hydroxydecanoyl chain.

In previous mutagenesis studies, the *E. coli* LpxA G173C and G173S mutants, like G173M, were found to be *R*-3-hydroxydecanoyl-ACP selective, but they were inactive with both *R*-3-hydroxymyristoyl-ACP and *R*-3-hydroxylauroyl-ACP (19). This anomaly is explained by the positioning of G173 relative to the bound acyl chain (Fig. 6). The side chains of serine and cysteine would protrude into the fatty acid binding groove (Fig. 6) and clash with the terminal methyl group of an *R*-3-hydroxylauroyl residue. On the basis of the structure of the LpxA/UDP-3-*O*-(*R*-3-hydroxymyristoyl)-GlcNAc complex, we suggest that H191 (Fig. 6) might be responsible for limiting the ability of *E. coli* LpxA to use acyl chains longer than 14 carbon atoms. In *Helicobacter*, H191 is replaced with arginine, but its side-chain is oriented differently (17), and this would not prevent utilization of *R*-3-hydroxypalmitoyl-ACP.

Discussion

Our crystal structures of the complexes of LpxA with UDP-3-*O*-(*R*-3-hydroxymyristoyl)-GlcNAc at 1.74 Å and with UDP-3-*O*-(*R*-3-hydroxydecanoyl)-GlcNAc at 1.85 Å provide glimpses of how LpxA interacts with lipids. These structures account for the extraordinary acyl chain selectivity of *E. coli* LpxA (Fig. 6), and they support the direct transfer mechanism for the acylation of the sugar nucleotide (Fig. 7), first deduced by site-directed mutagenesis (18). In both of our product complexes and in the recent 3.0-Å structure of LpxA with bound UDP-GlcNAc (27), the H125/NE2 atom is situated within hydrogen-bonding distance of the GlcNAc 3-*O* atom. LpxA functions via a general base mechanism (Fig. 7) in which H125 activates the glucosamine 3-OH group of UDP-GlcNAc (18), thus converting it into a better nucleophile. In our structures, H125/NE2 also is within hydrogen-bonding distance of the GlcNAc *O*-4 atom (Fig. 7; not shown in Fig. 4 for clarity), but the significance of this interaction is unclear. In the reverse direction, H125/NE2 would be expected to activate the SH group of ACP for attack on the ester-linkage of the hydroxyacyl chain, but our structures do not address this aspect of the mechanism. The conserved D126 side chain positions and/or stabilizes the H125 side chain by hydrogen bonding the ND1 proton (Fig. 7). On the basis of its positioning relative to the carbonyl oxygen of the acyl chain, from which it is separated by ≈3.32–3.35 Å, we propose that the backbone NH group of G143 functions as the oxyanion hole during catalysis (Figs. 4 and 7).

Because the reverse reaction catalyzed by LpxA (Fig. 1) requires UDP-3-*O*-(*R*-3-hydroxymyristoyl)-GlcNAc as the acyl donor and free ACP as the acyl acceptor (18), intact UDP-3-*O*-(*R*-3-hydroxymyristoyl)-GlcNAc and UDP-3-*O*-(*R*-3-hydroxydecanoyl)-GlcNAc are visualized in the active sites of the complexes (Fig. 2). Conserved LpxA residues (Figs. 4 and 7) participate in binding these lipid ligands and account for the substrate specificity of the enzyme. The LpxA residues that contact the (*R*-3-hydroxyacyl)-GlcNAc and the β-phosphate units are almost identical in both structures (Fig. 4). For instance, the side chains of H144 (Figs. 4 and 7) and K76 (omitted for clarity in Fig. 4) hydrogen-bond the GlcNAc 6-OH group; K76 also interacts with the GlcNAc *O*-5 atom (Fig. 7). The backbone NH group of L75 is hydrogen-bonded to the carbonyl oxygen of the acetyl group (Fig. 4). The H122/NE2

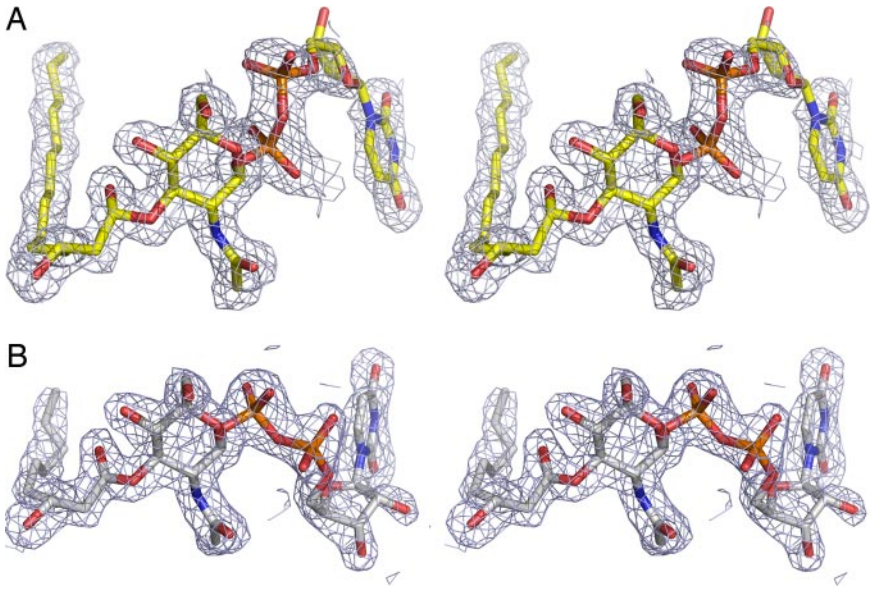

Fig. 3. Stereoviews of the electron densities of the bound ligands. (*A*) Stereoview of the final $2F_o - F_c$ electron density maps surrounding UDP-3-*O*-(*R*-3-hydroxymyristoyl)-GlcNAc contoured at 1.2 σ. (*B*) Stereoview of the final $2F_o - F_c$ electron density maps surrounding UDP-3-*O*-(*R*-3-hydroxydecanoyl)-GlcNAc contoured at 1.2 σ. The color scheme for the stick models of these ligands is the same as in Fig. 2.

atom hydrogen-bonds the *R*-3-OH moiety of the hydroxyacyl chain (Fig. 4). The *R*-3-OH group is further engaged by the side chain of Q73 and by a single, well defined water molecule (Figs. 4 and 7), which in turn is hydrogen-bonded to H99 (Figs. 4 and 7) and the backbone N of Q73 (omitted for clarity in Fig. 4). Interestingly, H99 is replaced by threonine in *C. trachomatis* LpxA (21). This substitution may account for loss of *R*-3-hydroxyacyl chain selectivity, because threonine cannot replace histidine as a hydrogen-bonding partner.

The conformation of the UDP moiety is distinctly different in the two complexes, arising from rotational reorientation of P–O bonds within the diphosphate unit (Fig. 5*A*). Whether or not the UDP binding mode seen with UDP-3-*O*-(*R*-3-hydroxymyristoyl)-GlcNAc contributes to the more efficient catalysis seen with 14-carbon *R*-3-hydroxyacyl chains is uncertain. The altered UDP conformation results in a significant redistribution of water molecules around the UDP moiety and changes its interactions with some LpxA side chains. A direct interaction between an α-phos-

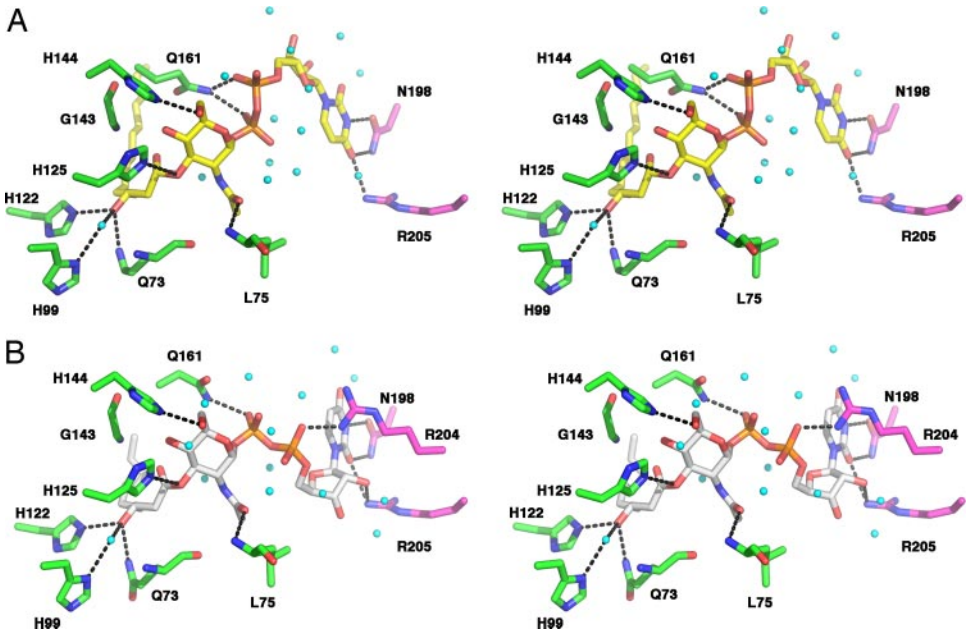

Fig. 4. Positioning of conserved residues within the active site of *E. coli* LpxA. (*A*) Stereoview of the interactions between residues in the active site of LpxA and UDP-3-*O*-(*R*-3-hydroxymyristoyl)-GlcNAc. The color scheme is the same as in Fig. 2. Water molecules are depicted as cyan spheres. Hydrogen bonds are represented as black dashed lines. Hydrogen bonds between water molecules and the product molecule were omitted for clarity. G134, the putative oxyanion hole, is slightly too far removed from the carbonyl group of the acyl chain for H-bonding (3.32–3.35 Å), but it might be able to interact during catalysis. (*B*) Stereoview of the interactions between LpxA and UDP-3-*O*-(*R*-3-hydroxydecanoyl)-GlcNAc. The color scheme is the same as in Fig. 2. The most significant differences are in the binding and orientation of the UDP moiety of the two ligands. In both structures, Q73 makes an additional hydrogen bond (not shown for clarity) via its backbone nitrogen atom to the single water molecule that is hydrogen-bonded to the R-3-OH moiety of the ligand.

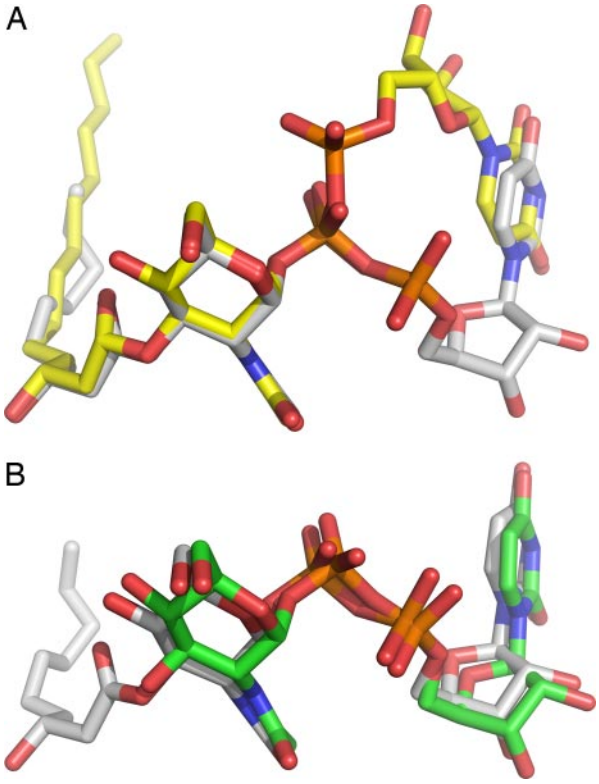

Fig. 5. Alternative conformations for the UDP moiety in LpxA/ligand complexes. (*A*) Superimposition of the ligands in the LpxA/UDP-3-*O*-(*R*-3-hydroxydecanoyl)-GlcNAc complex and the LpxA/UDP-3-*O*-(*R*-3-hydroxymyristoyl)-GlcNAc complex highlights the similarities and differences in the binding of the ligands. The positions of the atoms within the GlcNAc residue, the first four carbon and oxygen atoms of the acyl chain, and the β-phosphate group are positioned identically. However, the α-phosphate, the ribose ring, and the uracil moiety assume an entirely different orientation, which nevertheless permits the uracil moiety to hydrogen-bond to the side chain of N198 in both instances (Fig. 4). The color scheme is the same as in Fig. 2. (*B*) Superimposition of the ligands in the LpxA/UDP-3-*O*-(*R*-3-hydroxydecanoyl)-GlcNAc complex and the 3-Å LpxA/UDP-GlcNAc complex (27). Carbons of the latter ligand are green. The conformations of the GlcNAc and UDP moieties are virtually identical for these two complexes, showing that the presence of the longer *R*-3-hydroxymyristoyl chain exerts subtle effects on UDP binding.

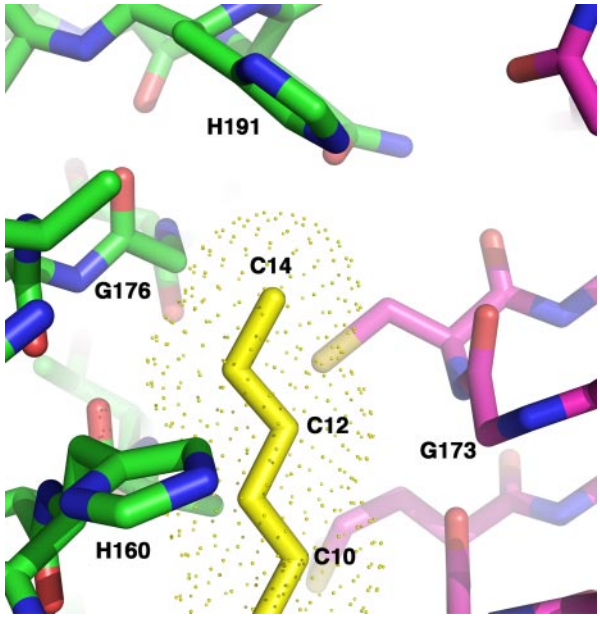

Fig. 6. Positioning of the end of the *R*-3-hydroxymyristoyl chain near G173. This view displays one of the three active sites of LpxA with bound UDP-3-*O*-(*R*-3-hydroxymyristoyl)-GlcNAc. The carbon atoms of the ligand (sticks with dots) are yellow, and the terminal methyl group (C14) is near the top, in the vicinity of H191. C12 of the *R*-3-hydroxymyristoyl chain is located in close proximity to G173. The terminal methyl group of the acyl chain of UDP-3-*O*-(*R*-3-hydroxydecanoyl)-GlcNAc (not shown) would be located between carbons 9 and 10 of UDP-3-*O*-(*R*-3-hydroxymyristoyl)-GlcNAc (Fig. 5*A*).

phate oxygen and R204, seen in the UDP-3-*O*-(*R*-3-hydroxydecanoyl)-GlcNAc complex (Fig. 4*B*), is lost when UDP-3-*O*-(*R*-3-hydroxymyristoyl)-GlcNAc is bound (Fig. 4*A*). However, a new hydrogen bond appears to be formed between this α-phosphate oxygen and the Q161/NE2 atom in the UDP-3-*O*-(*R*-3-hydroxymyristoyl)-GlcNAc complex (Fig. 4*A*). Despite the reversal of the uridine ring (Fig. 5), the side chains of N198 and R205 retain their ability to hydrogen-bond the base effectively (Fig. 4, compare *A* with *B*).

E. coli LpxA is specific for the UDP moiety of UDP-GlcNAc (6), and the reasons are now structurally apparent. The space in the UDP binding pocket of LpxA is sufficient to accommodate an analogue like TDP-GlcNAc, which is used at ≈20% of the rate of UDP-GlcNAc (6). Other nucleotide sugars, like ADP-GlcNAc and GDP-GlcNAc, are not substrates for LpxA (6), probably because of steric hindrance. CDP-GlcNAc is similar in size to UDP-GlcNAc but also is not a substrate for LpxA (6). Cytidine groups cannot always substitute for uridine, because of the differences in their hydrogen bonding capacity, which may be relevant in the case of LpxA (Figs. 4 and 7).

Previous studies implicated G173 as a "hydrocarbon ruler" that determines acyl chain length selectivity (19). We have now identified the fatty acid binding groove for *E. coli* LpxA (Figs. 2 and 6). In both complexes, the fatty acyl chain emerging from the sugar nucleotide initially lies perpendicular to the long axis of the β-helix, but it then turns and runs parallel to the helix (Figs. 2 and 5). The C12 acyl chain atom of UDP-3-*O*-(*R*-3-hydroxymyristoyl)-GlcNAc (Fig. 6) passes near G173, and the terminal methyl group (C14) is situated near H191 (Fig. 6). This arrangement is consistent with the finding that the G173M, G173F, G173S, and G173C substitutions do not use *R*-3-hydroxymyristoyl- or *R*-3-hydroxylauroyl-ACP, but instead display *R*-3-hydroxydecanoyl-ACP selectivity (Fig. 6) (19). The G173A mutant, although greatly reduced in activity, remains somewhat selective for *R*-3-hydroxymyristoyl-ACP (19), consistent with the structure (Fig. 6). Therefore, steric hindrance is probably the main reason for the altered acyl chain length selectivity of these mutants, but it may not be the only explanation. The active site of *E. coli* LpxA utilizes 14-carbon acyl chains two orders of magnitude faster than 12- or 16-carbon acyl chains and three orders of magnitude faster than 10-carbon acyl chains (19). Acyl chains that are shorter than 14 carbon atoms contribute less binding energy and therefore may be transferred at a slower rate. On the basis of the structure shown in Fig. 6, it should be possible to design further changes in the acyl chain selectivity of LpxA. For instance, *E. coli* LpxA might prefer a 16-carbon hydroxyacyl chain if H191 were replaced with alanine or arginine (as seen in *Helicobacter* LpxA) (17). Structures of LpxA orthologues with intrinsically different acyl chain selectivity, such as the C10-selective *P. aeruginosa* LpxA (31) or the C12-selective *Leptospira interrogans* LpxA (32), might provide further insights in the acyl chain recognition mechanism. *L. interrogans* LpxA displays the additional interesting feature of requiring as its acceptor substrate an analogue of UDP-GlcNAc, in which an amine replaces the GlcNAc *O*-3 atom (32, 33). *E. coli* LpxA utilizes both of these sugar nucleotides at comparable rates but cannot synthesize the analogue (32).

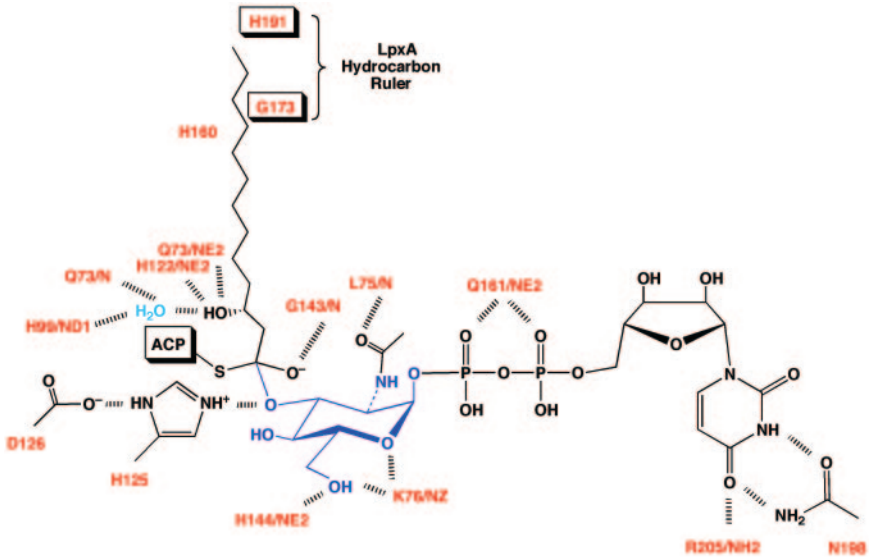

Fig. 7. Role of conserved LpxA residues in acyl chain selectivity and catalysis. Our structural analysis supports the previously proposed role of H125 as the catalytic base (18, 32) and further identifies the functions of various conserved side chains in substrate binding during the tetrahedral transition state, as indicated. Uncertainties remain about the positioning of the phosphopantetheine arm of ACP and the role of the conserved H160 residue (Fig. 6), the side chain of which is displaced by the presence of the acyl chain of the ligand. The proposed role of G143 as the oxyanion hole is inferred on the basis of the absolute conservation of this residue and its positioning near the carbonyl oxygen atoms of the ligands, as shown in Fig. 4.

There are no crystal structures of LpxA with bound acyl-ACP. A few crystal or NMR structures are available for *E. coli* ACP and acyl-ACP (34–37), but these do not provide definitive information about the location and conformation of the phosphopantetheine moiety. Modeling studies based on chemical shift perturbations of ^{15}N-labeled ACP in the presence of *E. coli* LpxA suggest that ACP docks in the vicinity of R204 (36). If the complex of LpxA and acyl-ACP cannot be crystallized, then crystals of LpxA with bound acyl-phosphopantetheine should be examined, because their structural analysis might provide insights into the positioning of the thioester group during catalysis in the forward direction.

E. coli LpxA is a validated target for antibiotic development (12, 28), but few potent inhibitors, other than peptide 920 (28), have been reported. Our product complex structures should facilitate the rational design of new inhibitors that target LpxA. Libraries of uridine analogues could be screened for initial leads (38). The recently reported structure of LpxD (Fig. 1) with bound UDP-GlcNAc (39) also may provide additional clues. The first six enzymes of the lipid A pathway (Fig. 1) are outstanding targets for new antibiotic discovery, and the crystal structures of the first three enzymes are now available with bound ligands and/or inhibitors (Fig. 8). These structures provide exciting insights into the emerging area of lipid/protein structural biology. Potent LpxC inhibitors with antibiotic activity comparable to ciprofloxacin have already provided the proof of principle (14), and should be useful for the treatment of infections caused by multidrug-resistant Gram-negative bacteria.

Materials and Methods

Reagents. Synthetic UDP-3-*O*-(*R*-3-hydroxy-decanoyl)-GlcNAc and synthetic UDP-3-*O*-(*R*-3-hydroxymyristoyl)-GlcNAc used

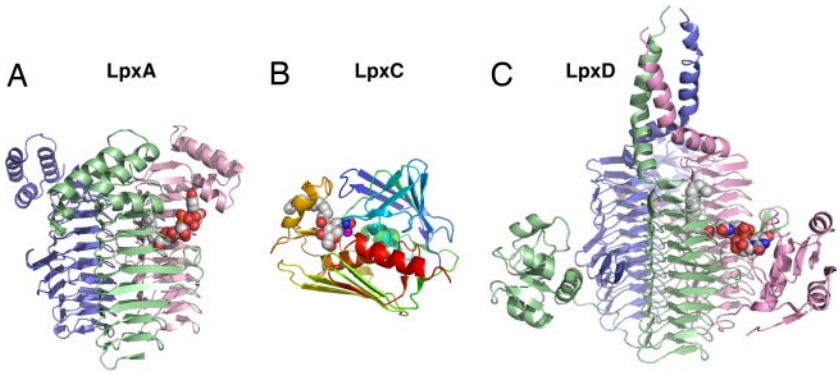

Fig. 8. Structures of the first three enzymes of the lipid A pathway with bound lipid ligands. (*A*) Crystal structure of *E. coli* LpxA with bound UDP-3-*O*-(*R*-3-hydroxydecanoyl)-GlcNAc, as determined in the present study; only one bound ligand is shown for clarity. (*B*) Representative NMR structure of *Aquifex aeolicus* LpxC with bound substrate-mimetic inhibitor TU514. The catalytic zinc atom is magenta. LpxC consists of a single polypeptide chain, colored with a gradient of colors (N terminus in blue to the C terminus in red). The acyl chain of the inhibitor is trapped within an unusual tunnel, which opens to solvent at the surface of the protein (48, 49). This structural feature explains why LpxC requires the presence of a 3-*O*-linked acyl chain in its substrate for activity and why LpxC is not very selective with regard to the length of that acyl chain. (*C*) Crystal structure of the trimeric *C. trachomatis* LpxD with bound UDP-GlcNAc and a free fatty acid (39), showing the similarity of the β-helix domain to that of LpxA and the location of one of the active sites. The natural LpxD acceptor substrate is UDP-3-*O*-(*R*-3-hydroxyacyl)-glucosamine. The locations of the acyl-ACP binding sites on LpxA and LpxD are unknown.

for crystallography were purchased from the Alberta Research Council (Edmonton, Canada).

Sample Preparation for Crystallization. *E. coli* LpxA was expressed and purified as previously described (8, 18, 40). Crystals of LpxA and product complexes were grown at 18°C by using the hanging drop vapor diffusion method (40). Concentrated solutions of UDP-3-*O*-(*R*-3-hydroxymyristoyl)-GlcNAc or UDP-3-*O*-(*R*-3-hydroxydecanoyl)-GlcNAc were added to separate solutions of concentrated LpxA (25 mg/ml) to yield a 25-fold molar excess over enzyme monomer. Individual droplets contained equal volumes of the LpxA and ligand solutions as well as 0.8–1.4 M Na/K phosphate, pH 5.6–6.3, as generated with Hampton Research (Aliso Viejo, CA) solution HR2–223, and 30–35% DMSO. Crystalline cubes grew to ≈0.6 mm after 5 days.

Data Collection. Crystals of the LpxA/UDP-3-*O*-(*R*-3-hydroxymyristoyl)-GlcNAc and the LpxA/UDP-3-*O*-(*R*-3-hydroxydecanoyl)-GlcNAc complexes were cryoprotected in 1.0–1.2 M Na/K phosphate, pH 6.0, and 32% DMSO, and then were flash frozen in liquid nitrogen. Diffraction data were collected on an R-Axis IV image plate detector. Crystals of LpxA with bound UDP-3-*O*-(*R*-3-hydroxymyristoyl)-GlcNAc diffracted to 1.74 Å and belonged to space group $P2_13$ ($a = b = c = 97.14$ Å). Crystals of LpxA with bound UDP-3-*O*-(*R*-3-hydroxydecanoyl)-GlcNAc diffracted to 1.85 Å and likewise belonged to space group $P2_13$ ($a = b = c = 96.72$ Å). In both structures, there was one protein molecule in the asymmetric unit, consisting of either one LpxA subunit in complex with one UDP-3-*O*-(*R*-3-hydroxymyristoyl)-GlcNAc molecule or one LpxA subunit in complex with one UDP-3-*O*-(*R*-3-hydroxydecanoyl)-GlcNAc molecule. The biologically functional trimer lies on a crystallographic threefold axis.

Structure Determination and Refinement. Diffraction images were reduced and scaled by using HKL2000 (41). Phases were determined by using molecular replacement with the program MolRep (42). The search model consisted of a single LpxA monomer from the earlier structure determination at 2.6 Å (Protein Data Bank ID code 1LXA) (16). Iterative rounds of model building were performed by using the programs O and Coot, with rounds of simulated annealing, energy minimization, and B-factor refinement in Refmac (a part of the CCP4 suite) (43–45). Identification of non-water solvent molecules was accomplished with iterative rounds of solvent identification in the program ARP/warp (46). The quality of the final model was assessed by using MolProbity and PROCHECK (30, 47). The figures were drawn using PyMOL (DeLano Scientific, San Carlos, CA). Data collection and refinement statistics are presented in Table 1.

We thank Drs. Jane Richardson and James Phillips of the Department of Biochemistry, Duke University Medical Center, for stimulating discussions and help with the structure analysis. This work was supported by National Institutes of Health Grant GM-51310 (to C.R.H.R.).

1. Rietschel ET, Kirikae T, Schade FU, Mamat U, Schmidt G, Loppnow H, Ulmer AJ, Zähringer U, Seydel U, Di Padova F, *et al.* (1994) *FASEB J* 8:217–225.
2. Raetz CRH, Whitfield C (2002) *Annu Rev Biochem* 71:635–700.
3. Raetz CRH, Garrett TA, Reynolds CM, Shaw WA, Moore JD, Smith DC, Jr, Ribeiro AA, Murphy RC, Ulevitch RJ, Fearns C, *et al.* (2006) *J Lipid Res* 47:1097–1111.
4. Raetz CRH, Reynolds CM, Trent MS, Bishop RE (2007) *Annu Rev Biochem*, 76:295–329.
5. Anderson MS, Bulawa CE, Raetz CRH (1985) *J Biol Chem* 260:15536–15541.
6. Anderson MS, Raetz CRH (1987) *J Biol Chem* 262:5159–5169.
7. Coleman J, Raetz CRH (1988) *J Bacteriol* 170:1268–1274.
8. Anderson MS, Bull HS, Galloway SM, Kelly TM, Mohan S, Radika K, Raetz CRH (1993) *J Biol Chem* 268:19858–19865.
9. Anderson MS, Robertson AD, Macher I, Raetz CRH (1988) *Biochemistry* 27:1908–1917.
10. Young K, Silver LL, Bramhill D, Cameron P, Eveland SS, Raetz CRH, Hyland SA, Anderson MS (1995) *J Biol Chem* 270:30384–30391.
11. Beall B, Lutkenhaus J (1987) *J Bacteriol* 169:5408–5415.
12. Galloway SM, Raetz CRH (1990) *J Biol Chem* 265:6394–6402.
13. Onishi HR, Pelak BA, Gerckens LS, Silver LL, Kahan FM, Chen MH, Patchett AA, Galloway SM, Hyland SA, Anderson MS, Raetz CRH (1996) *Science* 274:980–982.
14. McClerren AL, Endsley S, Bowman JL, Andersen NH, Guan Z, Rudolph J, Raetz CRH (2005) *Biochemistry* 44:16574–16583.
15. Mdluli KE, Witte PR, Kline T, Barb AW, Erwin AL, Mansfield BE, McClerren AL, Pirrung MC, Tumey LN, Warrener P, *et al.* (2006) *Antimicrob Agents Chemother* 50:2178–2184.
16. Raetz CRH, Roderick SL (1995) *Science* 270:997–1000.
17. Lee BI, Suh SW (2003) *Proteins* 53:772–774.
18. Wyckoff TJ, Raetz CRH (1999) *J Biol Chem* 274:27047–27055.
19. Wyckoff TJO, Lin S, Cotter RJ, Dotson GD, Raetz CRH (1998) *J Biol Chem* 273:32369–32372.
20. Williamson JM, Anderson MS, Raetz CRH (1991) *J Bacteriol* 173:3591–3596.
21. Sweet CR, Lin S, Cotter RJ, Raetz CRH (2001) *J Biol Chem* 276:19565–19574.
22. Beaman TW, Blanchard JS, Roderick SL (1998) *Biochemistry* 37:10363–10369.
23. Olsen LR, Roderick SL (2001) *Biochemistry* 40:1913–1921.
24. Wang XG, Olsen LR, Roderick SL (2002) *Structure (London)* 10:581–588.
25. Kisker C, Schindelin H, Alber BE, Ferry JG, Rees DC (1996) *EMBO J* 15:2323–2330.
26. Ning B, Elbein AD (2000) *Eur J Biochem* 267:6866–6874.
27. Ulaganathan V, Buetow L, Hunter WN (2007) *J Mol Biol* 369:305–312.
28. Williams AH, Immormino RM, Gewirth DT, Raetz CRH (2006) *Proc Natl Acad Sci USA* 103:10877–10882.
29. Benson RE, Gottlin EB, Christensen DJ, Hamilton PT (2003) *Antimicrob Agents Chemother* 47:2875–2881.
30. Davis IW, Murray LW, Richardson JS, Richardson DC (2004) *Nucleic Acids Res* 32:W615–619.
31. Dotson GD, Kaltashov IA, Cotter RJ, Raetz CRH (1998) *J Bacteriol* 180:330–337.
32. Sweet CR, Williams AH, Karbarz MJ, Werts C, Kalb SR, Cotter RJ, Raetz CRH (2004) *J Biol Chem* 279:25411–25419.
33. Sweet CR, Ribeiro AA, Raetz CRH (2004) *J Biol Chem* 279:25400–25410.
34. Kim Y, Prestegard JH (1990) *Proteins* 8:377–385.
35. Oswood MC, Kim Y, Ohlrogge JB, Prestegard JH (1997) *Proteins* 27:131–143.
36. Jain NU, Wyckoff TJ, Raetz CRH, Prestegard JH (2004) *J Mol Biol* 343:1379–1389.
37. Roujeinikova A, Baldock C, Simon WJ, Gilroy J, Baker PJ, Stuitje AR, Rice DW, Slabas AR, Rafferty JB (2002) *Structure (London)* 10:825–835.
38. Winans KA, Bertozzi CR (2002) *Chem Biol* 9:113–129.
39. Buetow L, Smith TK, Dawson A, Fyffe S, Hunter WN (2007) *Proc Natl Acad Sci USA* 104:4321–4326.
40. Pfitzner U, Raetz CRH, Roderick SL (1995) *Proteins Struct Funct Genet* 22:191–192.
41. Otwinowski Z, Minor W (1997) *Methods Enzymol* 276:307–326.
42. Vagin A, Teplyakov A (1997) *J Appl Crystallogr* 30:1022–1025.
43. Jones TA, Kjeldgaard M (1994) in *From First Map to Final Model*, eds Bailey S, Hubbard R, Waller D (Sci Eng Res Council Darebury Lab, Warrington, U.K.), pp 1–13.
44. Emsley P, Cowtan K (2004) *Acta Crystallogr D* 60:2126–2132.
45. Murshudov GN, Vagin AA, Dodson EJ (1997) *Acta Crystallogr D* 53:240–255.
46. Cohen SX, Morris RJ, Fernandez FJ, Ben Jelloul M, Kakaris M, Parthasarathy V, Lamzin VS, Kleywegt GJ, Perrakis A (2004) *Acta Crystallogr D* 60:2222–2229.
47. Lovell SC, Davis IW, Arendall WB, III, de Bakker PI, Word JM, Prisant MG, Richardson JS, Richardson DC (2003) *Proteins* 50:437–450.
48. Coggins BE, McClerren AL, Jiang L, Li X, Rudolph J, Hindsgaul O, Raetz CRH, Zhou P (2005) *Biochemistry* 44:1114–11126.
49. Gennadios HA, Whittington DA, Li X, Fierke CA, Christianson DW (2006) *Biochemistry* 45:7940–7948.